NANO LETTERS

Letter

pubs.acs.org/NanoLett

Oleic Acid-Induced Atomic Alignment of ZnS Polyhedral Nanocrystals

Ward van der Stam,[†] Freddy T. Rabouw,[†] Sander J. W. Vonk,[†] Jaco J. Geuchies,[†] Hans Ligthart,[†] Andrei V. Petukhov,[‡,§] and Celso de Mello Donega*[,†]

[†]Condensed Matter and Interfaces, Debye Institute for Nanomaterials Science, Utrecht University, P.O. Box 80000, 3508 TA Utrecht, The Netherlands

[‡]Physical and Colloid Chemistry, Debye Institute for Nanomaterials Science, Padualaan 8, 3584 CH Utrecht, The Netherlands

[§]Laboratory of Physical Chemistry, Department of Chemical Engineering and Chemistry, Eindhoven University of Technology, P.O. Box 513, 5600 MB Eindhoven, The Netherlands

Supporting Information

ABSTRACT: Ordered two-dimensional (2D) superstructures of colloidal nanocrystals (NCs) can be tailored by the size, shape, composition, and surface chemistry of the NC building blocks, which can give directionality to the resulting superstructure geometry. The exact formation mechanism of 2D NC superstructures is however not yet fully understood. Here, we show that oleic acid (OA) ligands induce atomic alignment of wurtzite ZnS bifrustum-shaped NCs. We find that in the presence of OA ligands the {002} facets of the ZnS bifrustums preferentially adhere to the liquid−air interface. Furthermore, OA ligands induce inter-NC interactions that also orient the NCs in the plane of the liquid−air interface, resulting in atomically aligned 2D superstructures. We follow the self-assembly process in real-time with in situ grazing incidence small-angle X-ray scattering and find that the NCs form a hexagonal superstructure at early stages after which they come closer over time, resulting in a close-packed NC superstructure. Our results demonstrate the profound influence that surface ligands have on the directionality of 2D NC superstructures and highlight the importance of detailed in situ studies in order to understand the self-assembly of NCs into 2D superstructures.

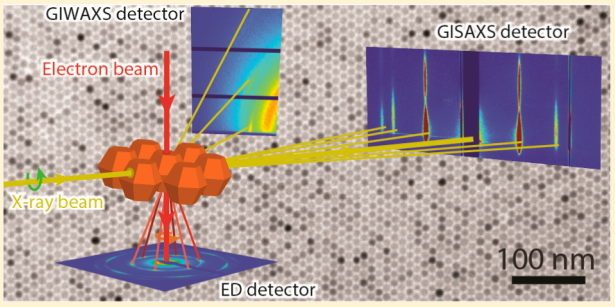

KEYWORDS: *Colloidal nanocrystals, surface ligands, self-assembly, atomic alignment, grazing incidence small-/wide-angle X-ray scattering*

Colloidal nanocrystals (NCs) are able to form three-dimensional (3D) and two-dimensional (2D) self-assembled superstructures with properties that are dictated not only by the size, shape, and composition of the building blocks but also by the geometry into which they self-assemble.[1−7] For example, the precise geometry can be important to the electrical transport properties of the superstructure[8] or to the directionality and polarization of emitted light.[4,6] Of key interest in this respect is the challenge of using the shape of the NC building blocks to program the final geometry of the superstructure.[9−15] Besides, controlling the inter-NC interactions with surface ligands has been shown to have a dramatic impact on the directionality of the self-assembly process.[9,16−20] However, the exact mechanisms underlying directional self-organization are not yet fully understood. In a previous study, we investigated the self-assembly of hexagonal bipyramid- and bifrustum-shaped ZnS NCs into 2D superlattices by using ex situ transmission electron microscopy (TEM) in combination with interfacial free-energy calculations and Monte Carlo simulations.[14] On the basis of our results, we proposed a mechanism for the self-assembly process in which the NCs are confined to the liquid−air interface due to an irreversible adsorption, after which they close-pack into shape-directed geometries (tetragonal for hexagonal bipyramids and hexagonal for bifrustums).[14] This mechanism, however, was not experimentally verified, because we carried out only ex situ TEM measurements. Moreover, we showed that the addition of surface ligands (e.g., dodecanethiol, DDT) disrupts the self-organization process but the role of the ligands was not investigated in detail.[14]

Here, we study in situ the influence of oleic acid (OA) ligands on the self-assembly of hexagonal bifrustum ZnS NCs into 2D superstructures by adding OA ligands prior to the onset of the self-organization process. The self-assembled 2D NC superstructures are obtained by the liquid substrate procedure in which a concentrated NC solution in toluene is drop-casted onto a dense liquid substrate (ethylene glycol, EG)[21] and is subsequently allowed to dry out over the course of

Received: January 18, 2016
Revised: February 26, 2016
Published: March 1, 2016

DOI: 10.1021/acs.nanolett.6b00221
Nano Lett. 2016, 16, 2608−2614

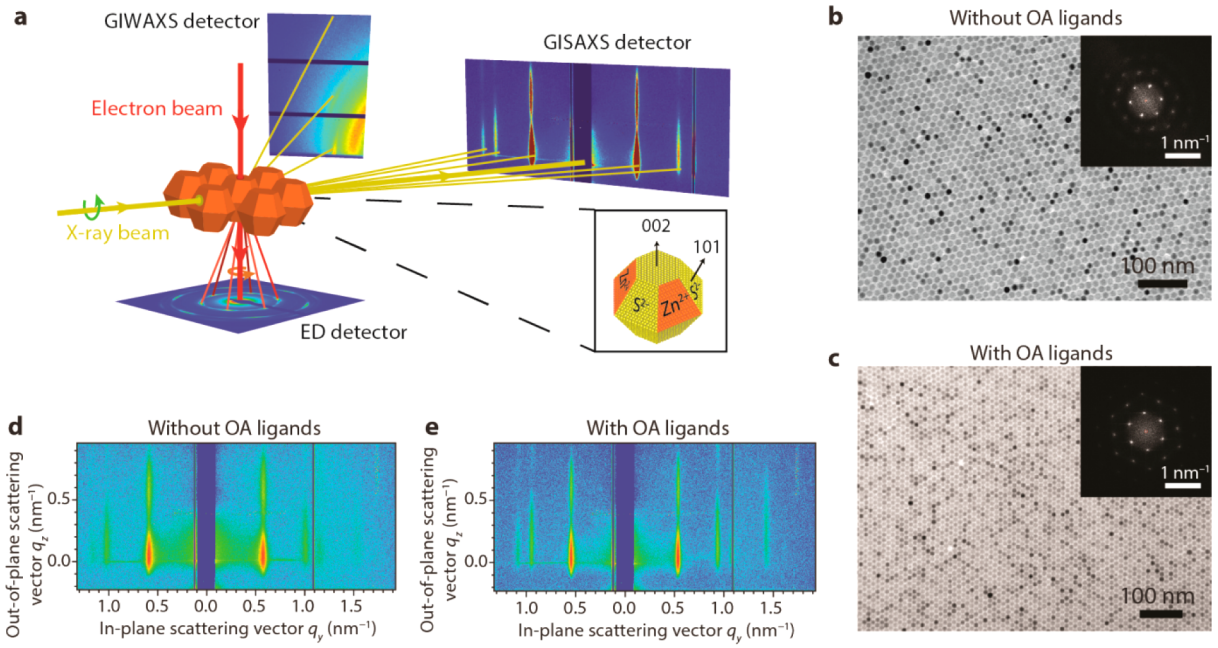

Figure 1. Schematic representation of the in situ GISAXS and GIWAXS measurements, the ex situ ED measurements, and the geometry of the wurtzite bifrustum-shaped ZnS NCs. (a) The 2D ZnS NC superstructures were studied in situ with GISAXS and GIWAXS, simultaneously, following the formation of the superlattice on nanocrystal and atomic length scales, respectively. Ex situ ED analysis reveals the atomic order. The combination of in situ GIWAXS and ex situ ED provides information about the orientation of the NCs with respect to the liquid−air interface (GIWAXS), as well as in the plane of the interface (ED). The inset shows an enlargement of the wurtzite hexagonal bifrustum-shaped ZnS NCs with two hexagonal {002} facets and 12 trapezoidal {101} facets. In a stoichiometric wurtzite ZnS NC, the {101} facets are alternating Zn- and S-terminated (orange area for Zn-terminated facets, inset). (b) Ex situ TEM analysis on 2D ZnS NC superstructures shows long-range NC order with hexagonal symmetry, as evidenced by the FFT (insets), with an interparticle spacing of 12.2 nm without the addition of OA ligands and (c) 13.6 nm with the addition of OA ligands. (d,e) Snapshot of the in situ GISAXS measurements during the formation of the 2D hexagonal 2D ZnS superstructure (t = 18 min) reveals hexagonal symmetry with scattering rods in the in-plane scattering direction at relative q-values of $1:\sqrt{3}:2:\sqrt{7}$ both (d) without and (e) with OA ligands added.

an hour (see Supporting Information, Experimental Section for details). A combination of in situ time-resolved grazing incidence small-angle X-ray scattering (GISAXS) and grazing incidence wide-angle X-ray scattering (GIWAXS) is used to selectively probe the liquid−air interface at both nanometer and atomic length scales, simultaneously, allowing the NC and atomic order to be followed in real-time during the whole self-assembly process. Furthermore, the resulting 2D NC superstructures are collected on a TEM-grid, and analyzed ex situ with TEM and electron diffraction (ED). We find that long-range hexagonal 2D ZnS NC superstructures are formed both in the absence and in the presence of OA ligands. However, in the presence of OA ligands the atomic planes of the wurtzite ZnS bifrustum-shaped NCs align themselves, forming an atomically ordered NC superlattice. These results highlight the huge impact of surface ligands on the directionality of the self-organization process, which may prove beneficial for the design of well-defined, high-quality 2D NC superstructures of various compositions.

The techniques used in our study give information about the positional order of the NCs in situ and ex situ (GISAXS and TEM, respectively, Figure 1a), the orientational order with respect to the liquid−air interface in situ (GIWAXS, Figure 1a), and the orientational order in the plane of the interface (ED, Figure 1a). The wurtzite ZnS NCs studied in this work have two distinct types of crystal facets (viz., two hexagonal {002} top and bottom facets and 12 trapezoidal {101} side facets, as displayed in the inset of Figure 1a). If we assume that the ZnS NCs are near-stoichiometric, then the {101} facets are alternatingly Zn- and S-terminated (Figure 1a). In this situation, both oleic acid (OA) and oleylamine (OLAM) ligands are expected to selectively bind to the Zn-terminated {101} facets,[22,23] because they are neutral Lewis bases (L-type ligands) and will therefore bind to Lewis acids (e.g., Zn^{2+}) but not to other Lewis bases (e.g., S^{2-}).[24] The native ligands on the ZnS NCs are OLAM molecules ($C_{18}H_{35}NH_2$), which bind to the surface Zn^{2+} atoms through the donor N atom of the amine headgroup.[23] The added OA ligands ($C_{17}H_{33}COOH$) are expected to replace the OLAM ligands via a ligand exchange reaction, because their carboxylic acid headgroup coordinates more strongly to Zn^{2+} than amine groups due to its bidentate character and the harder Lewis base nature of the O donor atoms.[23,24] Moreover, the added OA ligands are in excess with respect to the native OLAM ligands (lower limit estimate for the OA/surface Zn sites ratio is 350, see Supporting Information, Experimental Section for details). The self-assembly of the hexagonal bifrustum ZnS NCs (diameter: 11 nm) was investigated with and without adding OA to the EG substrate prior to the addition of the NC solution (see Supporting Information, Experimental Section for details). Ex situ TEM analysis of the resulting NC superstructures shows long-range NC order over several square micrometers, encompassing several thousands of NCs, both in the presence and in the absence of OA (Figure 1b,c). FFT analysis shows hexagonal NC order and an interparticle separation of 12.2 nm without added OA ligands (inset Figure 1b) and 13.6 nm with added OA ligands (inset Figure 1c). OLAM and OA have comparable chain lengths (viz., 2 nm)[25] and a double bond

DOI: 10.1021/acs.nanolett.6b00221
Nano Lett. 2016, 16, 2608−2614

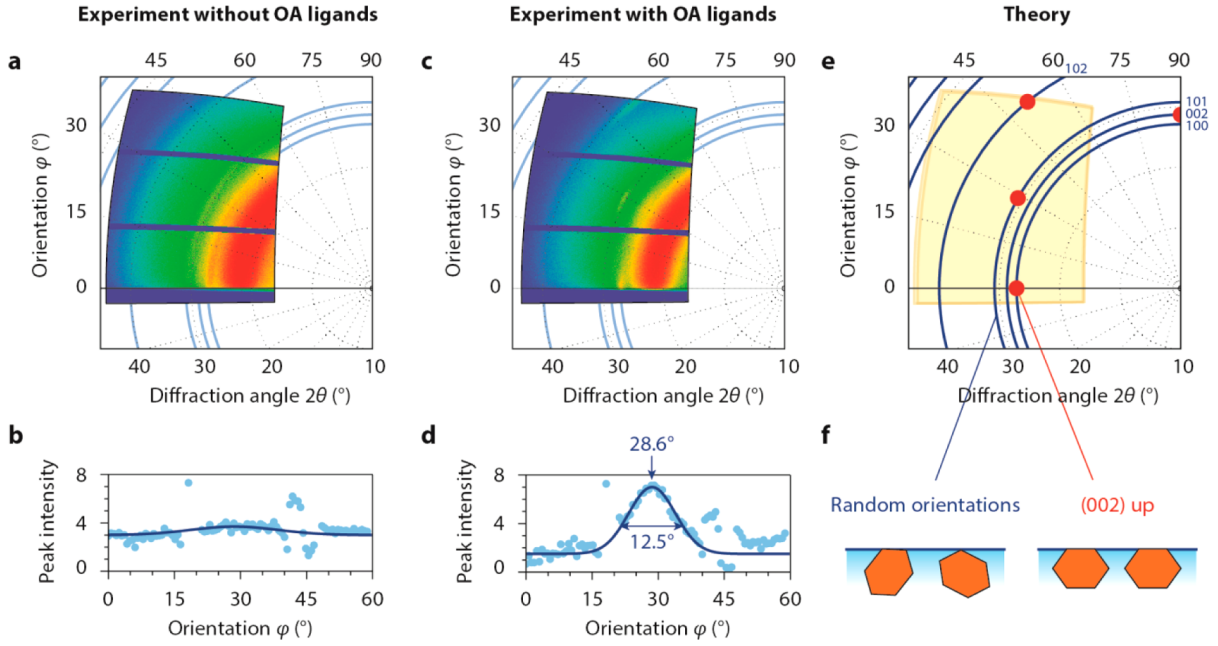

Figure 2. Oleic acid induced atomic alignment. (a) GIWAXS analysis of wurtzite ZnS 2D NC superstructures shows that in the absence of OA ligands, the NCs adsorbed at the liquid−air interface have full rotational freedom, evidenced by diffraction rings in the GIWAXS pattern. The broad intense scattering signal at small 2θ originates from the EG liquid substrate. (b) The intensity profile of the {101} reflection as a function of azimuthal angle φ reveals no orientation in the absence of OA ligands. (c) In the presence of OA ligands, the {100}, {101}, and {102} reflections are concentrated into well-defined spots, indicating atomic alignment. (d) In the presence of additional OA ligands, the intensity profile of the {101} reflection as a function of azimuthal angle φ reveals that the {101} reflections are oriented at 28.6° with respect to the toluene−air interface, indicating that the {002} facets are pointing upward. The NCs have a 12.5° distribution in orientation (full width at half-maximum). (e) Calculated GIWAXS pattern for wurtzite ZnS NCs with the (002) facet pointing upward (red dots). (f) Schematic representations of two hexagonal bifrustum ZnS NCs adhered to the toluene−air interface with random orientations, resulting in diffraction rings (left) and with their {002} facets pointing upward, resulting in well-defined diffraction spots (right).

between C9 and C10, differing only with respect to the headgroup (i.e., NH_2 and COOH, respectively). Therefore, the observed increase in interparticle separation in the presence of OA ligands cannot be explained by an increase in chain length due to OLAM for OA ligand exchange. However, as mentioned above, OA is a stronger and less dynamic ligand than OLAM[23,26,27] and therefore the ligand coverage density of the Zn-terminated {101} facets of the NCs has likely increased due to the addition of OA ligands, which prevents the ligands to fully interdigitate,[15] resulting in larger interparticle separations.

Hexagonal NC order is also evident from snapshots of the in situ GISAXS measurements (Figure 1d,e; t = 18 min in both cases). Scattering rods in the in-plane scattering direction are observed at relative q-values of $1:\sqrt{3}:2:\sqrt{7}$, which are characteristic for hexagonal 2D supercrystals (Figure 1d,e).[9,28,29] From the scattering rods, nearest-neighbor interparticle separations of 11.2 nm (without OA ligands) and 11.5 nm (with OA ligands) were deduced at the end of the experiment (t = 60 min). The discrepancy between the inter-NC separation deduced from in situ (viz., 11.2 and 11.5 nm, without and with OA, respectively) and ex situ (viz., 12.2 and 13.6 nm, without and with OA, respectively) measurements will be discussed in more detail below.

The difference between the superstructures formed in the presence or absence of OA ligands becomes apparent from the GIWAXS patterns. In the absence of OA, the GIWAXS signal shows rings (Figure 2a,b), indicating that the NCs have full rotational freedom at the liquid−air interface. In the presence of OA ligands, the atomic scattering is focused into spots (Figure 2c,d), which clearly demonstrates that the NCs adsorb with a preferred crystallographic orientation. The atomic {100}, {101}, and {102} crystal planes scatter at well-defined azimuthal angles φ, from which the NC orientation at the liquid−air interface can be deduced. For example, the orientation of the {101} reflection is 28.6° with respect to the plane of the superstructure with 12.5° orientation distribution (Figure 2d). This indicates that the {002} facets are pointing upward. In fact, the experimental GIWAXS pattern, obtained in the presence of OA ligands, closely matches the simulated pattern for NCs adsorbed with a {002} facet at the liquid−air interface (Figure 2e,f). Wurtzite ZnS NCs adhered to the liquid−air interface with their {101} facets generate diffraction spots at different azimuthal angles φ, as experimentally verified by assembling hexagonal ZnS bipyramidal NCs (diameter, 28 nm; length, 38 nm) and larger hexagonal ZnS bifrustum NCs (diameter, 33 nm) (Supporting Information, Figure S1). The assembly of larger ZnS bifrustums (diameter, 33 nm) into 2D superstructures shows both orientations, that is, {002} and {101} facets pointing upward (Figure S1). Presumably, this indicates that an increase in facet area, due to an increase in size of the entire NC, creates two deep local minima for the adsorption of the NCs to the air−toluene interface, which is in agreement with the theoretical calculations reported in our previous work.[14] Furthermore, we note that we also investigated the influence of additional DDT and OLAM ligands on the self-assembly of ZnS NCs and found that DDT disrupts the 2D self-assembly (i.e., results in 3D superstructures), whereas additional OLAM has no influence

DOI: 10.1021/acs.nanolett.6b00221
Nano Lett. 2016, 16, 2608−2614

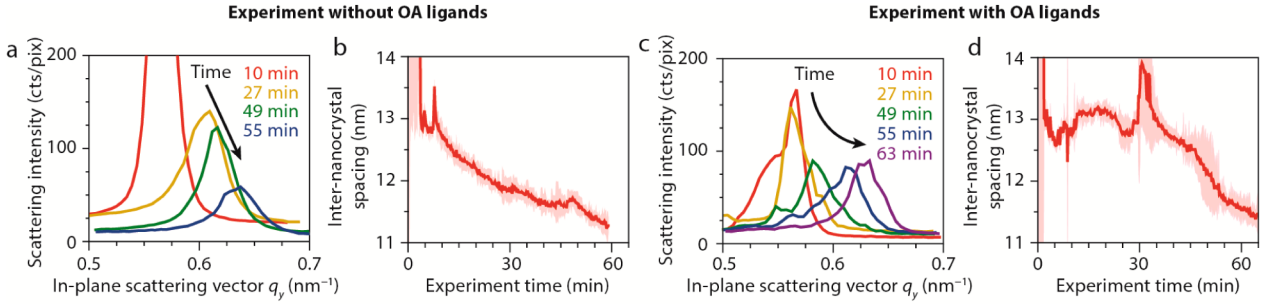

Figure 3. GISAXS analysis of 2D ZnS NC hexagonal superstructures. Time-resolved GISAXS measurements show a shift of the diffraction rods to larger in-plane scattering vectors, indicating a reduction in interparticle separation, that is, shrinking of the superstructure without (a,b) and with (c,d) the addition of OA ligands. (a,c) A zoom of the first scattering rod clearly shows the shift during the first hour, indicating that the NCs, while ordered, come closer together. The final in-plane nearest-neighbor distance in the 2D superstructure is (b) 11.2 ± 0.2 nm without OA ligands added and (d) 11.5 ± 0.2 nm with OA ligands.

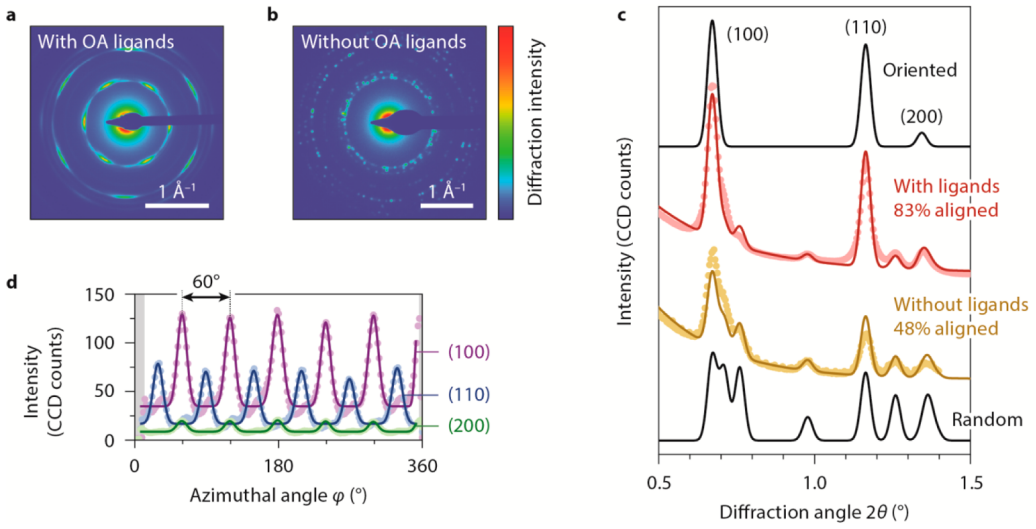

Figure 4. Ex situ ED measurements on 2D ZnS NC superstructures. (a) ED pattern of 2D superstructure in the presence of OA ligands, showing preferred orientation, evidenced by diffraction spots. (b) ED pattern of 2D superstructure in the absence of OA ligands, showing random orientation, evidenced by diffraction rings. (c) By integration of the 2D ED pattern in (a,b), the 1D diffraction line profile is obtained. In the presence of OA, the {100} and {110} reflections have increased intensity (compare red data points to yellow data points), consistent with {002} facets pointing upward. The black lines are the expected ED patterns (based on the known XRD pattern of PDF-card no. [05-0492] and Debye−Scherrer equation for wurtzite ZnS NCs with a diameter of 11 nm) for randomly oriented NCs (bottom) and NCs oriented with the 002 axis upward (top). The solid red and yellow lines are fits to a combination of aligned and randomly oriented NCs. We find that 48% of the NCs is aligned without additional OA ligands (yellow line), but after the addition of OA ligands this value is 83%. (d) ED intensity profiles as a function of azimuthal angle, for the {100} (purple dots), {110} (blue dots), and {200} (green dots) reflections, showing 6-fold symmetry, indicating preferred orientation in the *xy*-plane.

on the formation of 2D superstructures or on the atomic alignment of individual NCs.

Time-resolved GISAXS measurements of the NC ordering shows a shift of the scattering rods to larger q-values during the evaporation of the solvent toluene, as evidenced by the temporal evolution of the first scattering peak around 0.6 nm^{-1} (Figure 3a,b, see also supporting discussion and Figure S2). This implies that the NCs come closer together in real space, that is, the superstructure shrinks over time. The shifts of the scattering peaks in the GISAXS signal over the course of the entire experiment (duration, 60 min) are displayed in Figure 3c,d. This shows that the NCs order at the interface into a hexagonal structure already at early stages (t = 5 min) of the self-assembly process. Gradually, the interparticle separation is reduced, presumably as more NCs adhere to the 2D interface. Eventually, this results into ordered close-packed 2D hexagonal superstructures with in-plane nearest-neighbor distances of 11.2 ± 0.2 nm without OA ligands added and 11.5 ± 0.2 nm with OA ligands added (the error is given as the standard deviation in nearest-neighbor distances calculated from the first- and higher-order scattering rods at both sides of the beam stop). These in-plane nearest-neighbor distances are 1−2 nm shorter than observed ex situ by TEM (viz., 12.2 and 13.6 nm without and with OA ligands added, respectively, see above), and very close to the diameter of the NCs (11 nm).

The surprisingly close in-plane NC separation observed in situ and the discrepancy between the in situ and ex situ inter-NC separations can be explained in two ways. First, if we assume that the 2D plane of self-assembled NCs at the air−toluene interface is buckled (i.e., some NCs are pushed out of the plane, either up or down), the interparticle separation can be theoretically reduced from 13.6 nm (completely planar structure) to 10.4 nm (maximum buckling), even if the surface-to-surface distance is fixed at 2 nm by the ligand layers (Supporting Information, Figure S3). Considering that no additional peaks are observed in the GISAXS patterns, the

DOI: 10.1021/acs.nanolett.6b00221
Nano Lett. 2016, 16, 2608−2614

buckling would have to be aperiodic. Buckling has been previously observed for 2D superstructures, such as honeycomb superlattices with a silicene-like structure, formed by oriented attachment of PbSe NCs.[9] The PbSe NCs are atomically attached and therefore the buckled structure is mechanically stable and can be observed with TEM.[9] In the present case, however, the in-plane NC separation observed with ex situ TEM is larger than that observed in situ. This can be ascribed to the fact that the ZnS NCs are not attached, so that the buckled superstructure is allowed to relax back to the planar superstructure under influence of the strong capillary forces acting during drying of the ZnS NC superstructures prior to TEM imaging. Alternatively, the in situ surface coverage with OA ligands may be relatively low and therefore the ligands have rotational freedom on the NC surface, resulting in a ligand layer of ~0.5 nm. Hanrath and co-workers have recently shown with molecular dynamics that at low surface coverage of PbSe NCs with OA ligands inter-NC separations as small as 0.5 nm are indeed possible.[22] In this scenario, the larger interparticle separation observed ex situ could be explained by assuming that the surface coverage density by OA ligands increases during drying of the ZnS superstructures due to binding of OA ligands originally in solution.

As depicted in Figure 1a, preferred orientation of atomic planes can be observed in situ with GIWAXS and ex situ with ED. The two techniques reveal the degree of atomic orientation of the NCs in two different directions, namely the extent of rotational disorder in the plane perpendicular to the respective incoming beam (i.e., X-ray beam and electron beam). This is indicated in Figure 1a with the circled arrows. GIWAXS shows how strictly the NCs are adsorbed at the liquid−air interface with a particular facet adhered, as discussed above (Figure 3). ED shows not only how the NCs are adsorbed to the interface but also how they are oriented in the 2D plane. Diffraction only occurs on planes oriented along the electron beam. In the case of NCs with a [002] axis pointing upward (i.e., with OA added), we therefore mainly see {100}, {110}, and {200} reflections (Figure 4a). Furthermore, the ED pattern is 6-fold rotationally symmetric, which proves that the NCs have a preferred atomic orientation in the 2D plane. Such preferred orientation is absent when no OA ligands were added. Instead, disordered spots on vague rings are observed, consistent with random orientation of ZnS NCs (Figure 4b). From the radially integrated 1D ED patterns with OA ligands (red data points in Figure 4c), it is directly evident that the {002} facets are pointing upward, because this reflection (which would be at $2\theta = 0.78°$) is almost absent in the integrated diffraction profile. The fraction of aligned and random NCs can be calculated by comparing the intensities of the different reflections. To this end, the integrated 1D ED patterns were fitted to the known XRD pattern of wurtzite ZnS (JCPDS-card no. [05-0492]) with the width of the peaks set by the Debye−Scherrer equation for NCs with a diameter of 11 nm. This analysis reveals that without OA ligands added, 48% of the NCs are oriented with their {002} facet pointing upward (yellow line in Figure 4c), whereas in the presence of OA ligands, 83% of the NCs are aligned (red line in Figure 4c). The ED intensity profiles as a function of azimuthal angle φ of the {100} (purple dots in Figure 4d), {110} (blue dots in Figure 4d), and {200} (green dots in Figure 4d) reflections show 6-fold symmetry because of preferred orientation in the *xy*-plane. As expected, the {100} and {200} diffraction spots occur at the same azimuthal angle (with a variation in orientation of $\sigma = 6.2°$) and the reflections are separated by 60°, whereas the {110} reflection is 30° out-of-phase with the {100} and {200} reflections (Figure 4d).

The in situ GISAXS and GIWAXS experiments in combination with ex situ TEM analysis have provided us a full picture of the self-assembly process, including the effect of OA ligands. The first step of the self-assembly process is the adhesion of the NCs to the air−toluene interface (step 1, Figure 5a). Theoretical calculations have shown that this step is irreversible.[14] The experimental results discussed above show that in the absence of OA ligands the adhesion of 11 nm diameter ZnS bifrustum NCs to the interface occurs randomly without any preferential orientation. However, in the presence of OA ligands, the ZnS NCs preferentially adhere to the air−toluene interface with their {002} facets. This can be understood by assuming that the OA ligands selectively bind to the trapezoidal Zn-terminated {101} facets of the ZnS bifrustums. The polar {002} facets are either Zn- or S-terminated, and therefore at least one of them (i.e., the S-terminated) would be free of capping ligands. Selective binding of OA to the {101} facets would thus make their free-energy lower than that of the {002} facets. Consequently, the {002} facets adhere to the liquid−air interface to minimize the NC−toluene interfacial tension. As a result, the NCs are confined to the interface with a fixed orientation and are only allowed to rotate and translate in the plane of the interface.[14] During the evaporation of the toluene, the NCs are forced to close-pack into hexagonal 2D superstructures (step 2, Figure 5b). In the absence of OA ligands, the NCs also form hexagonal 2D superstructures, but the atomic planes of the building blocks are randomly oriented with respect to each other (Figure 5d), as the NCs are still allowed to rotate in the plane. In the presence of OA ligands, the NCs are atomically aligned. We propose that this alignment is due to directional interactions between the OA ligands bound to the {101} facets (Figure 5c,e). The {101} facets are alternatingly Zn- and S-terminated and the added OA ligands are expected to selectively bind to the Zn-terminated {101} facets.[23,24] This results in three {101} facets above the hexagonal base capped with OA ligands and three {101} facets below the hexagonal base. A second NC with the same surface coverage can then rotate such that its "bare" S-terminated {101} facet orients to a fully covered Zn-terminated {101} facet (Figure 5c,e). This limits the rotational freedom of the NCs, resulting in preferred orientation of the atomic planes, because the {002} facet is already locked at the air−toluene interface.

In conclusion, we have shown that oleic acid (OA) ligands induce atomic alignment of hexagonal bifrustum-shaped wurtzite ZnS NCs in hexagonal 2D superstructures. GIWAXS and ED show that the {002} facets of the ZnS NCs preferentially adhere to the air−toluene interface in the presence of OA ligands, resulting in atomic alignment. This is ascribed to directional interactions between the NCs when confined to the *xy*-plane after adhesion, thereby limiting their in-plane rotational freedom. Our results highlight the importance of surface chemistry control on the design of ordered and atomically aligned NC superstructures and show that the impact of ligands on the directionality of the self-organization process strongly depends not only on the morphology and faceting of the NC building blocks but also on the chemical composition of the exposed facets and on the interaction between ligands. The approach described here can thus potentially be extended to other polyhedral shapes. Furthermore, our findings may prove beneficial for applications in the field of photovoltaic and plasmonic devices in which

DOI: 10.1021/acs.nanolett.6b00221
Nano Lett. 2016, 16, 2608−2614

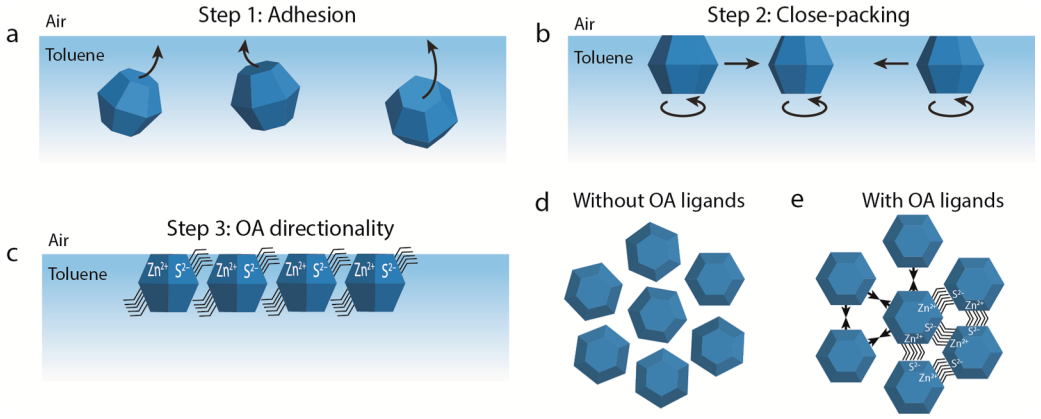

Figure 5. Schematic representation of the formation mechanism of 2D ZnS nanocrystal superstructures. (a) Step 1: The hexagonal bifrustum-shaped ZnS NCs adhere preferentially with their {002} facets to the air−toluene interface in the presence of OA ligands. (b) Step 2: After this adhesion, the NCs approach each other while confined to the interface and can only translate and rotate in the plane of the interface. (c) Step 3: OA ligands give directionality to the self-organization process by selectively adhering to the Zn-terminated {101} facets. (d) In the absence of OA ligands, the NCs can rotate in the plane of the interface without preferred orientation of the NCs. (e) The addition of OA ligands increases the surface coverage of the Zn-terminated {101} facets and therefore limits the rotational freedom of the NCs, resulting in preferred orientation of the atomic planes at the liquid−air interface.

ordered thin layers are crucial for optimal charge injection and carrier mobility.[8,30−33]

■ ASSOCIATED CONTENT

Supporting Information

The Supporting Information is available free of charge on the ACS Publications website at DOI: 10.1021/acs.nanolett.6b00221.

Experimental section. TEM, GISAXS, GIWAXS, calculated diffraction pattern of hexagonal bipyramidal ZnS NCs, and hexagonal bifrustum ZnS NCs, supporting discussion, schematic representation of GISAXS corrections, and schematic representation of buckling at the air−toluene interface. (PDF)

■ AUTHOR INFORMATION

Corresponding Author

*E-mail: c.demello-donega@uu.nl.

Notes

The authors declare no competing financial interest.

■ ACKNOWLEDGMENTS

The measurements were performed at the ID10 beamline at ESRF, Grenoble. The authors thank Oleg Konovalov and Federico Zontone for support during the synchrotron experiments and for valuable discussions. W.v.d.S. and C.d.M.D acknowledge financial support from the division of Chemical Sciences (CW) of The Netherlands Organization for Scientific Research (NWO) under Grant ECHO.712.012.001.

■ REFERENCES

(1) Vanmaekelbergh, D. *Nano Today* **2011**, *6*, 419−437.
(2) Cargnello, M.; Diroll, B. T.; Gaulding, E. A.; Murray, C. B. *Adv. Mater.* **2014**, *26*, 2419−2423.
(3) Reifsnyder, D. C.; Ye, X.; Gordon, T. R.; Song, C.; Murray, C. B. *ACS Nano* **2013**, *7*, 4307−4315.
(4) Wang, T.; Zhuang, J.; Lynch, J.; Chen, O.; Wang, Z.; Wang, X.; LaMontagne, D.; Wu, H.; Wang, Z.; Cao, Y. C. *Science* **2012**, *338*, 358−363.
(5) Vanmaekelbergh, D.; van Vugt, L. K.; Bakker, H. E.; Rabouw, F. T.; De Nijs, B.; van Dijk-Moes, R. J. A.; van Huis, M. A.; Baesjou, P. J.; van Blaaderen, A. *ACS Nano* **2015**, *9*, 3942−3950.
(6) Abécassis, B.; Tessier, M. D.; Davidson, P.; Dubertret, B. *Nano Lett.* **2014**, *14*, 710−715.
(7) Cargnello, M.; Johnston-Peck, A. C.; Diroll, B. T.; Wong, E.; Datta, B.; Damodhar, D.; Doan-Nguyen, V. V. T.; Herzing, A. A.; Kagan, C. R.; Murray, C. B. *Nature* **2015**, *524*, 450−453.
(8) Evers, W. H.; Schins, J. M.; Aerts, M.; Kulkarni, A.; Capiod, P.; Berthe, M.; Grandidier, B.; Delerue, C.; van der Zant, H. S. J.; van Overbeek, C.; Peters, J. L.; Vanmaekelbergh, D.; Siebbeles, L. D. A. *Nat. Commun.* **2015**, *6*, 8195−8203.
(9) Boneschanscher, M. P.; Evers, W. H.; Geuchies, J. J.; Altantzis, T.; Goris, B.; Rabouw, F. T.; Van Rossum, S. A. P.; Van Der Zant, H. S. J.; Siebbeles, L. D. A.; Van Tendeloo, G.; Swart, I.; Hilhorst, J.; Petukhov, A. V.; Bals, S.; Vanmaekelbergh, D. *Science* **2014**, *344*, 1377−1381.
(10) Ye, X.; Chen, J.; Engel, M.; Millan, J. A.; Li, W.; Qi, L.; Xing, G.; Collins, J. E.; Kagan, C. R.; Li, J.; Glotzer, S. C.; Murray, C. B. *Nat. Chem.* **2013**, *5*, 466−473.
(11) Miszta, K.; de Graaf, J.; Bertoni, G.; Dorfs, D.; Brescia, R.; Marras, S.; Ceseracciu, L.; Cingolani, R.; van Roij, R.; Dijkstra, M.; Manna, L. *Nat. Mater.* **2011**, *10*, 872−876.
(12) Pietra, F.; Rabouw, F. T.; Evers, W. H.; Byelov, D. V.; Petukhov, A. V.; de Mello Donegá, C.; Vanmaekelbergh, D. *Nano Lett.* **2012**, *12*, 5515−5523.
(13) Bian, K.; Choi, J. J.; Kaushik, A.; Clancy, P.; Smilgies, D.-M.; Hanrath, T. *ACS Nano* **2011**, *5*, 2815−2823.
(14) van der Stam, W.; Gantapara, A. P.; Akkerman, Q. A.; Soligno, G.; Meeldijk, J. D.; van Roij, R.; Dijkstra, M.; de Mello Donega, C. *Nano Lett.* **2014**, *14*, 1032−1037.
(15) Choi, J. J.; Bian, K.; Baumgardner, W. J.; Smilgies, D.-M.; Hanrath, T. *Nano Lett.* **2012**, *12*, 4791−4798.
(16) Wang, Z.; Schliehe, C.; Bian, K.; Dale, D.; Bassett, W. A.; Hanrath, T.; Klinke, C.; Weller, H. *Nano Lett.* **2013**, *13*, 1303−1311.
(17) Choi, J. J.; Bealing, C. R.; Bian, K.; Hughes, K. J.; Zhang, W.; Smilgies, D.-M.; Hennig, R. G.; Engstrom, J. R.; Hanrath, T. *J. Am. Chem. Soc.* **2011**, *133*, 3131−3138.
(18) Nagaoka, Y.; Chen, O.; Wang, Z.; Cao, Y. C. *J. Am. Chem. Soc.* **2012**, *134*, 2868−2871.
(19) Yu, Y.; Goodfellow, B. W.; Rasch, M. R.; Bosoy, C.; Smilgies, D.-M.; Korgel, B. A. *Langmuir* **2015**, *31*, 6924−6932.
(20) Goodfellow, B. W.; Yu, Y.; Bosoy, C. A.; Smilgies, D.-M.; Korgel, B. A. *J. Phys. Chem. Lett.* **2015**, *6*, 2406−2412.
(21) Dong, A.; Chen, J.; Vora, P. M.; Kikkawa, J. M.; Murray, C. B. *Nature* **2010**, *466*, 474−477.

DOI: 10.1021/acs.nanolett.6b00221
Nano Lett. 2016, 16, 2608−2614

(22) Treml, B. E.; Lukose, B.; Clancy, P.; Smilgies, D.-M.; Hanrath, T. *Sci. Rep.* **2014**, *4*, 6731−6737.
(23) Donega, C. d. M. *Chem. Soc. Rev.* **2011**, *40*, 1512−1546.
(24) Pearson, R. G. *Inorg. Chem.* **1988**, *27*, 734−740.
(25) Wang, Z.; Wen, X.-D.; Hoffmann, R.; Son, J. S.; Li, R.; Fang, C.-C.; Smilgies, D.-M.; Hyeon, T. *Proc. Natl. Acad. Sci. U. S. A.* **2010**, *107*, 17119−17124.
(26) Fritzinger, B.; Capek, R. K.; Lambert, K.; Martins, J. C.; Hens, Z. *J. Am. Chem. Soc.* **2010**, *132*, 10195−10201.
(27) Hassinen, A.; Moreels, I.; de Mello Donegá, C.; Martins, J. C.; Hens, Z. *J. Phys. Chem. Lett.* **2010**, *1*, 2577−2581.
(28) Pietra, F.; Rabouw, F. T.; Van Rhee, P. G.; Van Rijssel, J.; Petukhov, A. V.; Erne, B. H.; Christianen, P. C. M.; de Mello Donega, C.; Vanmaekelbergh, D. *ACS Nano* **2014**, *8*, 10486−10495.
(29) Heitsch, A. T.; Patel, R. N.; Goodfellow, B. W.; Smilgies, D.-M.; Korgel, B. A. *J. Phys. Chem. C* **2010**, *114*, 14427−14432.
(30) Ip, A. H.; Thon, S. M.; Hoogland, S.; Voznyy, O.; Zhitomirsky, D.; Debnath, R.; Levina, L.; Rollny, L. R.; Carey, G. H.; Fischer, A.; Kemp, K. W.; Kramer, I. J.; Ning, Z.; Labelle, A. J.; Chou, K. W.; Amassian, A.; Sargent, E. H. *Nat. Nanotechnol.* **2012**, *7*, 577−582.
(31) Ginger, D. S.; Greenham, N. C. *J. Appl. Phys.* **2000**, *87*, 1361−1368.
(32) McDonald, S. A.; Konstantatos, G.; Zhang, S.; Cyr, P. W.; Klem, E. J. D.; Levina, L.; Sargent, E. H. *Nat. Mater.* **2005**, *4*, 138−142.
(33) Kim, G.-H.; Garcia de Arquer, F. P.; Yoon, Y. J.; Lan, X.; Liu, M.; Voznyy, O.; Yang, Z.; Fan, F.; Ip, A. H.; Kanjanaboos, P.; Hoogland, S.; Kim, J. Y.; Sargent, E. H. *Nano Lett.* **2015**, *15*, 7691−7696.

DOI: 10.1021/acs.nanolett.6b00221
Nano Lett. 2016, 16, 2608−2614